Journal of
Composites Science

MDPI

Article

Processing and Mechanics of Aromatic Vitrimeric Composites at Elevated Temperatures and Healing Performance

Tanaya Mandal [1], Unal Ozten [2], Louis Vaught [3], Jacob L. Meyer [4], Ahmad Amiri [5,6], Andreas Polycarpou [3,5] and Mohammad Naraghi [2,*]

[1] Department of Materials Science & Engineering, Texas A&M University, College Station, TX 77843, USA; tmandal90@tamu.edu
[2] Department of Aerospace Engineering, Texas A&M University, College Station, TX 77843, USA; uozten@tamu.edu
[3] J. Mike Walker '66 Mechanical Engineering Department, Texas A&M University, College Station, TX 77843, USA; lovaught@tamu.edu (L.V.); andreas-polycarpou@utulsa.edu (A.P.)
[4] ATSP Innovations, Houston, TX 77055, USA; jacob.l.meyer@atspinnovations.com
[5] Russell School of Chemical Engineering, The University of Tulsa, Tulsa, OK 74104, USA; ahmad-amiri@utulsa.edu
[6] Department of Mechanical Engineering, The University of Tulsa, Tulsa, Oklahoma 74104, USA
* Correspondence: naraghi@tamu.edu

Abstract: Carbon fiber reinforced polymer (CFRP) composites are renowned for their exceptional mechanical properties, with applications in industries such as automotive, aerospace, medical, civil, and beyond. Despite these merits, a significant challenge in CFRPs lies in their repairability and maintenance. This study, for the first time, delves into the processing and self-healing capability of aromatic thermosetting co-polyester vitrimer-based carbon fiber composites through mechanical testing. Vitrimers are an emerging class of thermosetting polymers, which, owing to their exchangeable covalent bonds, enable the re-formation of bonds across cracks. The specific vitrimer chosen for this study is an aromatic thermosetting co-polyester (ATSP). The mechanical properties of samples were analyzed initially through three-point bending (3PB) testing at room temperature before and after healing (by curing samples for 2 h at 280 °C). Samples were also 3PB tested at 100 °C to analyze their mechanical properties at an elevated temperature for comparison to the samples tested at room temperature. To investigate the fracture properties, optical microscopy images of samples were taken after 3PB tests, which were analyzed to observe crack initiation and crack growth behavior. Through load–displacement curves from double cantilever beam (DCB) mechanical testing, the Mode I crack initiation fracture toughness values of self-healed composites and control composites were calculated to evaluate healing efficiency in ATSP CFRP composites cured at 280 °C for 2 h. Scanning electron microscopy (SEM) showed a similar surface morphology of cracks before and after self-healing. Micro-computed tomography (CT) X-ray imaging confirmed that the healed samples closely resembled the as-fabricated ones, with the exception of some manufacturing voids, caused by outgassing in the initial healing cycle. This research demonstrated the ability for the in situ repair of ATSP CFRPs by restoring the fracture toughness to values comparable to the pristine composite (~289 J/m^2).

Keywords: carbon fibers; polymer matrix composites; aromatic thermosetting co-polyester; vitrimers; self-healing

Citation: Mandal, T.; Ozten, U.; Vaught, L.; Meyer, J.L.; Amiri, A.; Polycarpou, A.; Naraghi, M. Processing and Mechanics of Aromatic Vitrimeric Composites at Elevated Temperatures and Healing Performance. *J. Compos. Sci.* **2024**, *8*, 252. https://doi.org/10.3390/jcs8070252

Academic Editor: Jiadeng Zhu

Received: 24 May 2024
Revised: 20 June 2024
Accepted: 27 June 2024
Published: 1 July 2024

1. Introduction

Carbon fiber reinforced polymers (CFRPs) are highly desired in many fields including automotive, aerospace, and medical industries due to their exceptional mechanical properties, such as high elastic modulus and mechanical strength (as high as 1200–2410 MPa). These properties often exceed those of traditional engineering materials such as steel and aluminum, while offering the advantages of lower mass density and remarkable corrosion resistance [1–7]. In

a polymer-based composite, the matrix is a thermoset or thermoplastic [8–10]. Thermoset matrices contain polymer chains connected by strong covalent bonds, forming a network structure post-curing, offering enhanced thermal stability and strength [7,11–14]. Therefore, thermosets are extensively used in various sectors, including aerospace and wind energy [7,11–13].

Although thermoset composites have desirable properties, a main challenge is maintenance and repair, which is required upon the formation of microcracks, for instance, due to cyclic loading and fatigue damage, especially in aerospace epoxies [14–17]. In contrast, cracks in thermoplastics can heal by means of chain reconfiguration with heat, allowing dispersive bond reformation when crack faces are brought together above their glass transition temperature (T_g) [14,18].

Numerous studies have achieved self-healing in thermoset composites via incorporating microcapsules or microvascular networks to deliver healing agents into cracks after ruptured as well as self-healing intrinsic reactions in composites [19–28]. Microcapsule-based strategies include utilizing encapsulated healing agents such as ruthenium-based catalysts (Grubb's catalyst, G3) with 5-ethylidenenorbornene/dicyclopentadiene (ENB/DCPD) microcapsules [24–31], which demonstrated a 50% healing efficiency [24]. Although self-healing occurs through these microcapsule strategies, challenges persist such as monitoring the full use of healing agents and addressing insufficient microcapsule integration, resulting in partial self-healing. To combat this issue, Dry et al. developed a self-healing strategy involving microvascular networks, which embed liquid healing agents in hollow fiber or tubes. These methods increased the content of liquid healing agent that is injected into the samples' crack planes [32–35]. Some approaches use larger channels filled with resin, while others use smaller glass fibers filled with a cyanoacrylate resin to both heal and support the structure [36–38]. These techniques can restore ~97% of a material's flexural strength [23,38–44]. However, microvascular networks have disadvantages such as the need for low-viscosity resin to facilitate fiber infiltration and thermal strains in the composite due to thermal expansion coefficient mismatches. Moreover, given the much wider diameter of the microvascular tubes, the presence of the tubes required the removal of a large number of fibers, thereby diminishing the performance of the as-fabricated composites.

To address these challenges, it is desired for the thermoset matrix to exhibit reversible interchain bonding capability. This property enables damage repair similar to thermoplastics. To integrate these features, reformable covalent bonds are incorporated into the matrix, allowing thermoset network reconfiguration. In the 1990s, Economy's research group pioneered thermoset polymers with plasticity and adhesive bond formation across interfaces from bond exchange reactions [45,46]. From epoxy resins containing polyester bonds, Leibler et al. drew an analogy to glass by naming thermosets possessing exchangeable bonds as vitrimers [14,47]. Vitrimers' network structures can be reversible at/above certain temperatures depending on chemical composition [14,46]. Prior to crosslink formation, vitrimers exhibit viscous properties ~T_g according to Arrhenius' law [48,49]. At around the so-called freezing transition temperature (Tv), reversible reactions occur at labile sites, enabling self-healing and thermoplastic-like behavior [50–53].

Vitrimers, which can be utilized as a matrix material in CFRPs, should also demonstrate enhanced mechanical strength and retain bond exchange capability through covalent adaptable networks such as transesterification [53–55]. Transesterification exchanges bonds between beta-hydroxyls and esters cause epoxy precursor reactions with acids or anhydrides. Transesterification can be accelerated by metal-containing compound catalysts, such as zinc catalysts, which modulate epoxy resin reactivity through ligand exchange, causing anhydride ring-opening β-hydroxyl ester chain formation, resulting in monoester and carboxylic acid production [4]. In one study, diglycidyl ether (DGEBA) epoxy resin was treated with glutaric anhydride treatment. These samples underwent two different cure cycles: 180 °C for 4 h and 200 °C for 4 h. After DCB testing and healing, samples cured at 200 °C exhibited higher healing efficiency (~80%), compared to ~65% for samples cured at 180 °C [55]. In another study, a vitrimeric epoxy system was synthesized using

DGEBA and AV5 (1:1 epoxy/acyl ratio with 5% zinc acetate catalyst). DCB tests showed a decrease in G_{IC} for AV5 samples compared to epoxy resin A samples. Furthermore, lap shear tests on AV5 samples heated to ~200 °C revealed an ~84% healing efficiency [54]. These vitrimeric composites are desirable due to their recyclability, repairability, and reprocessability. Challenges include depolymerization and repolymerization as a self-healing mechanism to maintain composite integrity, especially at high temperatures >300 °C. Vitrimers withstanding high temperatures and maintaining integrity are sought to address these challenges.

One particularly high-performing vitrimer, which contains an effective combination of thermoset and thermoplastic properties, is known as aromatic thermosetting co-polyester (ATSP) [56]. ATSP contains crosslinked aromatic polyester oligomers, which have two oligomer types: those with acetoxy end groups (A-type) and those with carboxylic end groups (C-type). The oligomer combinations can include CB2AB2 and C1A1, derived from oligomer types such as C1, CB, A1, and AB, where B is derived from bisphenol diacetate. The ATSP family of vitrimers has notable properties such as self-healing, high T_g (174–310 °C), and resistance to high temperatures (>300 °C) [57,58]. The self-healing mechanism in ATSP is activated by interchain transesterification reactions when ATSP reaches temperatures > T_g [15,57–60]. These curing reactions involve covalent bond exchange between two thermoset ATSP sheets by reversible bonding through acidolysis and esterolysis with acetic acid by-products [57,61]. Uniquely, among published vitrimeric materials, ATSP resins are all fully aromatic thermosets—giving them very high T_g values among vitrimers. Additionally, their potential for strong liquid crystalline character, as introduced by their aromatic polyester repeat units, introduces characteristics, advantages, and challenges not typically seen in vitrimers [6].

Previous experimentation demonstrated that ATSP has minimal moisture absorption, similar to epoxy resins, and enhanced thermal stability, which is comparable to high-performing thermoset polyimides [62–64]. ATSPs have easier repairability than both polyimide and epoxy materials. ATSP is stable in air at 350 °C and also surpasses the decomposition thresholds temperature of most thermally stable epoxies in air (~170–190 °C) [65,66]. ATSPs have increased durability from physical aging since the moisture pickup of ATSP is low (0.3 wt%) compared to polyimides (2.6%) and epoxy (2.3%) [64–66]. These ATSP properties are desirable for high-temperature applications such as tribology, aerospace, oil and gas, and automotive industries [59,67,68].

In the present study, CB2AB2 ATSP was used as the matrix material to create CFRP composites to evaluate ATSP's self-healing properties on pre-notched samples and bending coupons. The CB2AB2 resin was chosen from the studied ATSP-type resins due to its lowest T_g within the family (174 °C) and because it was previously studied for its effective reversible bonding performance on metallic adherends. These characteristics suggest that it would perform well as the CFRP's matrix phase [58,61]. For the pre-notched samples, CFRPs were DCB-tested before and after self-healing to evaluate healing efficiency after a cure cycle. Based on load–displacement curves from DCB testing, the Mode I crack initiation fracture toughness (G_{IC}) and healing efficiency of ATSP CFRPs were calculated. Morphological analysis from SEM imaging and micro–CT X-ray imaging of the crack surfaces for both the as-fabricated ATSP CFRP samples and self-healed samples show evidence of similar surface morphology. In addition, 3PB testing of CFRPs was conducted to analyze mechanical properties at room temperature before and after self-healing at 280 °C for 2 h based on fracture mechanism behavior. The ATSP CFRP samples exhibited reduced fiber failure due to fiber sliding in 3PB testing conducted at room temperature before and after healing.

2. Experimental Section

2.1. Materials

The vitrimer used in this study was CB2AB2 ATSP, which was supplied by ATSP Innovations (Houston, TX, USA). N-methyl-2-pyrrolidone (NMP) was purchased from Millipore

Sigma (Burlington, MA, USA). Unidirectional carbon fiber sheets (12K unidirectional carbon fiber fabric, 95% carbon; Fiber Glast, Brookville, OH, USA) were used for composite fabrication.

2.2. ATSP CFRP Composite Processing

Composites were fabricated by first coating unidirectional carbon fiber sheets (12K unidirectional carbon fiber fabric, 95% carbon; Fiber Glast, Brookville, OH, USA) with ATSP and NMP, using a convection oven and a hot press. Eight 254 mm × 254 mm carbon fiber sheets were coated with a mixture of ATSP (CB2AB2) and NMP. The ATSP (density: 1.32 g/cm^3) and NMP were stirred via magnetic stir bar for 24 h at 400 rpm at room temperature. This mixture was then sonicated for 30 min and then magnetically stirred at 900 rpm at 90 °C for 24 h. The ATSP/NMP mixture was applied to each carbon fiber sheet with a roller and spreader. Sixteen sheets were placed in an oven to evaporate the NMP at 60 °C for 12 h. These sheets were then partially cured in the oven at 230 °C for 1 h followed by 260 °C for 1 more hour. After the partial cure to form the thermoset network from ATSP in the carbon fiber sheets, the sheets were cut into thirty-two 127 mm × 254 mm sheets. In preparation of hot pressing these sheets, an aluminum plate was prepared with a release layer of aluminum foil sheet, and sixteen carbon fiber sheets were placed on top. Six 63.5 mm aluminum foil sheets (three sheets at each end for DCB sample preparation) were placed between the two middle plies to maintain the pre-crack regions of the composite panel. The pre-crack dimensions were selected as per ASTM 5528 standards. The remaining sixteen carbon fiber sheets were then positioned, followed by the placement of another aluminum plate on top, and underwent hot pressing at 330 °C for 1 h under 5 MPa. This completed the composite laminate configuration of $[0]_{16s}$. The samples were removed from the hot press to cool, demolded, and cut into fourteen pieces via computer numerical control (CNC) (Mega V Router; Mill Right CNC, Leesburg, GA, USA) and a band saw. T-shaped sample grip fixtures were made from aluminum and fitted with aluminum rods. The grips were designed and cut from an aluminum plate. To prepare the samples for DCB testing, grip fixtures were fitted with resin glue on the pre-cracked end of the samples. ATSP CFRP samples with attached grip fixtures were fitted in the sample grip fixtures for DCB testing. A schematic of the procedure to construct ATSP CFRP samples is illustrated in Figure 1.

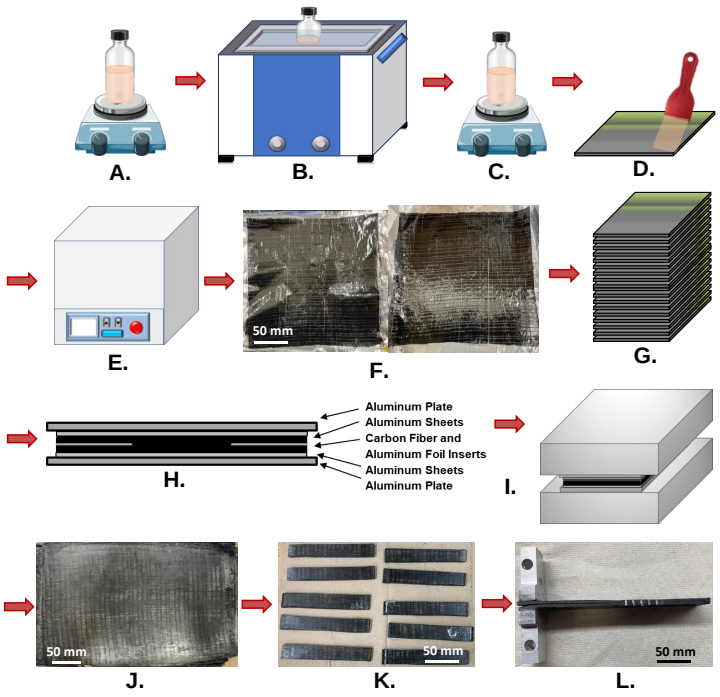

Figure 1. Schematic of ATSP CFRP composite processing is shown. (**A**–**C**). NMP-ATSP solution was obtained through a series of magnetic stirring and sonication. (**D**). The solution was spread onto

carbon fiber sheets. (**E**). Coated carbon sheets were cured in the oven. (**F**). ATSP-coated cured sheets were taken out of the oven. (**G**). Coated cured sheets were laid up. (**H**). The carbon fiber sheets, aluminum foil sheets, aluminum foil inserts, and aluminum plates were laid up for hot pressing. (**I**). The sample was hot-pressed. (**J**). The completed ATSP CFRP panel was removed from the hot press. (**K**). The panel was cut into fourteen samples. (**L**). Grip fixtures were glued to samples for DCB testing.

2.3. Sample Preparation and Mechanical Characterization of the Composites

For the three-point bending (3PB) tests, the composite panel was cut into samples for three-point bend (3PB) testing with dimensions of ~63 mm × 12.50 mm × 2.5 mm. The 3PB testing was performed at 1 mm/min using the ASTM 7264 standard with a gauge length of ~48 mm in two different temperature conditions: room temperature and 100 °C. A minimum of three tests were performed per case. To evaluate the ability of the material to recover from plastic deformations, the 3PB tests were carried out in a displacement-controlled mode, and the displacement was continued beyond the peak load, followed by unloading. The mechanical properties of the samples, namely the flexural strength and modulus, was compared between the samples tested at room temperature and elevated temperature to evaluate the effect of thermally induced softening and the viscoelastic behavior of the matrix on the overall mechanical properties of the composites.

Next, we utilized the exchangeable bonds in the matrix to recover the initial unbent shape of the 3PB tested samples. To this end, the plastically bent samples were heated in the oven at 280 °C for 2 h by clamping them between two aluminum plates under ~0.03 MPa. This temperature was selected to be considerably above the vitrification temperature to accelerate the healing of the samples. These samples were then retested at room temperature to compare and evaluate the extent to which the mechanical properties of the unbent samples were recovered. The room temperature samples underwent two healing cycles and retested for 3PB testing at room temperature. Flexural strength, modulus, and maximum strain were calculated after 3PB testing.

The flexural strength (σ) was calculated by using Equation (1), where P is applied force (N), L is gauge length (mm), b is width (mm), and h is thickness (mm):

$$\sigma = \frac{3PL}{2bh^2} \tag{1}$$

The flexural secant modulus of elasticity (E_f^{secant}) was calculated by using Equation (2), where m is the slope of the secant of the force–displacement curve.

$$E_f^{secant} = \frac{L^3 m}{4bh^3} \tag{2}$$

Moreover, the maximum strain experienced by the sample at the peak load (ε_{max}) during the 3PB test was calculated by Equation (3)

$$\varepsilon_{max} = \frac{6\delta h}{L^2} \tag{3}$$

2.4. Double Cantilever Beam Testing (DCB) and Self-Healing Cure Cycles

The DCB test was performed on ATSP CFRPs following the ASTM 5528 standards at a strain rate of 5 mm/min with a 2.5 kN load cell (MTS Systems Corporation, Eden Prairie, MN, USA) on the MTS Insight electromechanical tester machine (MTS Systems Corporation, Eden Prairie, MN, USA). The dimensions of each sample were 127 mm × 20.27 mm × 2.78 mm. The samples were secured by using pneumatic grips powered by compressed air on the sample grips holding the grip fixtures. During DCB testing, crack growth was measured optically by video recording the crack propagation so that data retrieval and video were concurrent. Crack length, a, was measured as the horizontal distance from the T bars to the end of the pre-crack region (Figure 2).

The DCB tests were run on each sample before and after healing (cure) cycles. Based on the test and healing procedure, the four samples were DCB-tested initially and then samples were cured at 280 °C for 2 h and cooled for 1 h. For the cure cycle, the samples with propagated cracks were placed between two aluminum plates wrapped in aluminum foil and secured by a clamp. Each sample was then self-healed in a Vulcan oven at 280 °C for 2 h and cooled for 1 h by clamping a sample between two aluminum plates under ~0.03 MPa. Following the cure cycles, the samples were tested again. Load–displacement data were recorded during the DCB tests to extract fracture toughness. The DCB experimental setup is shown in Figure 2.

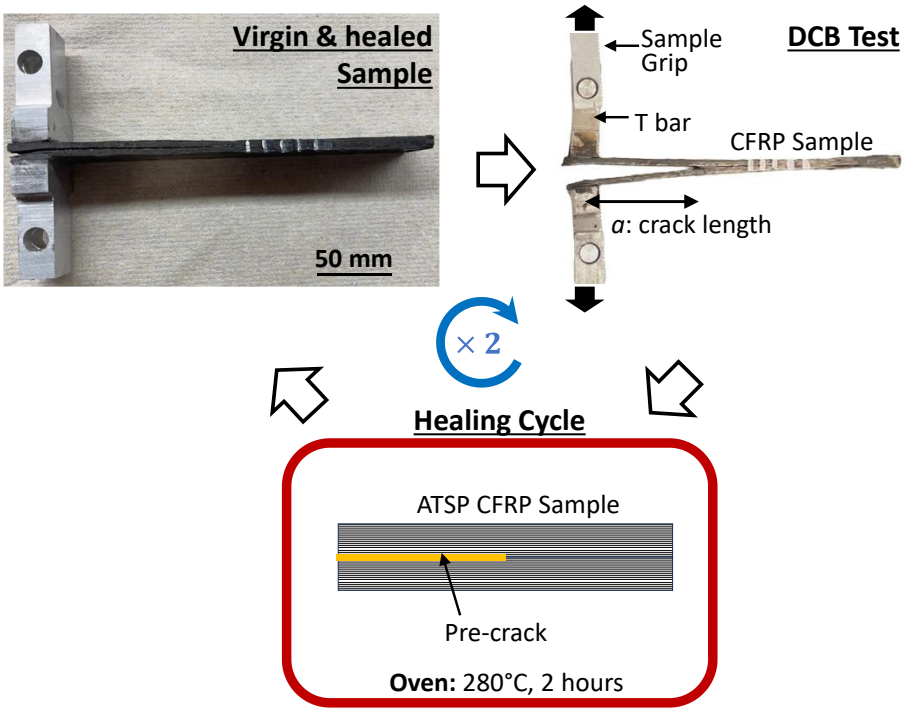

Figure 2. The virgin composite is first subjected to DCB test, followed by self-healing cycle and a subsequent DCB test to characterize the performance of the healed sample relative to the virgin material.

2.5. Measurement of Mode I Fracture Toughness and Healing Efficiency

The load–displacement data were then used to calculate Mode I interlaminar fracture toughness, G_{IC} (J/m^2), by using Equation (4), where ΔU is change in internal work (N mm), b is width (mm), a is crack length (mm), P is the load at crosshead displacement (N), δ is the displacement (mm), w is width (mm), and a is crack length (mm):

$$G_{IC} = \frac{1\Delta U}{b\Delta a} \text{ where } \Delta U = \int_0^{\delta} Pd\delta|_{\Delta a'} \quad (4)$$

where P and δ were obtained from the DCB testing, and b was measured for each sample [69]. a was acquired optically from the video of the crack growth. The G_{1C} was calculated for all samples before healing (virgin sample) and after self-healing (healed sample) and denoted as $G_{IC\text{-}v}$ and $G_{IC\text{-}h}$, respectively. The healing efficiency (H) of the ATSP CFRP samples was assessed by dividing the G_{IC} value before self-healing ($G_{IC\text{-}v}$) by the G_{IC} of the sample after self-healing ($G_{IC\text{-}h}$), as presented in Equation (5) [24]:

$$H(\%) = \frac{G_{IC-h}}{G_{IC-v}} \times 100 \quad (5)$$

The "area" approach laid out in Equation (4) to calculate the fracture toughness from DCB tests, unlike other methods, such as the "compliance" method, does not require compliance corrections based on the "true" value of the crack length [70]. Therefore, even

though it cannot be used to obtain an R-curve by calculating values of G_{IC} at different crack lengths, it is commonly used in the self-healing literature [71].

2.6. Material Characterization

A V2 Teledyne Lumenera INFINITY Optical Microscope was used to image the crack and fracture surface morphology of the 3PB samples before and after each healing cycle. An FEI Quanta 600 Field Emission Scanning Electron Microscope was used to image the surface morphology of the cracked surface of the samples before and after self-healing. Micro-CT X-ray imaging, utilizing the North Star Imaging (NSI) X50 X-ray/CT, was used to examine the internal structural morphology of ATSP CFRP samples before and after self-healing.

3. Results and Discussion

3.1. Identification of the Vitrification Temperature

To determine the temperature conducive to the healing process, we initially assessed the vitrification temperature of the polymer. The vitrification temperature, T_v, represents the lower temperature threshold at which healing may take place, with the option of employing higher temperatures to expedite the healing process. Traditionally, the vitrification temperature for self-healing thermosets is analyzed via either a fixed-displacement stress relaxation analysis or a fixed-load creep study. These methods determine the temperature at which the material begins to undergo plastic flow, representing a macroscale response that corresponds to molecular bond exchange behavior. For both the CB2AB2 material and ATSP copolyester vitrimers, analysis via these methods is obfuscated by significant viscoelastic response. Previous studies into the wear performance of materials within this family have shown significant elastic recovery via indentation testing [72–74]. As such, to confidently demonstrate the presence of self-healing behavior within the material, a cyclic creep test methodology was developed using a 30 min on–off loading cycle at 20 °C temperature increments and a loaded stress of 100 kPa. This procedure follows a prior study, which used a similar methodology to demonstrate self-healing but not to precisely determine the vitrification temperature [74]. Testing was performed using a PerkinElmer DMA 8000 in tensile mode, with a grip spacing of 10 mm; the raw test data are shown in Figure 3A and can be interpreted directly by noting trends in residual displacement after the material is relaxed. Under this testing regime, the material exhibited residual deformation until 140 °C, followed by recovery to an amount of permanent deformation that falls within the measurement error of the machine by 180 °C, indicating T_v = ~160–180°C, highlighted in Figure 3B.

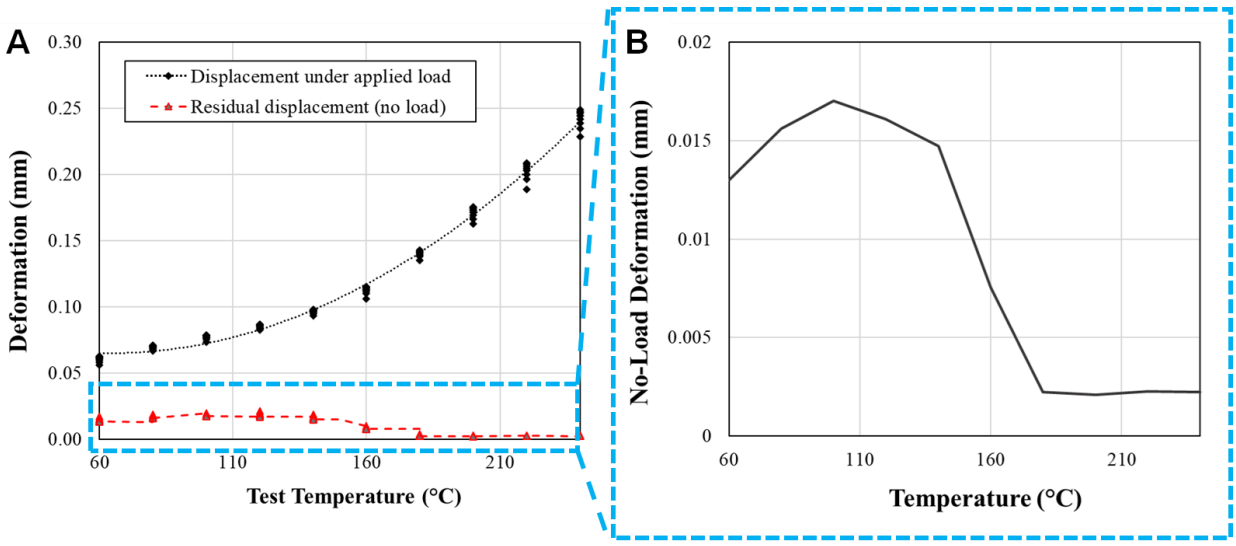

Figure 3. Vitrification temperature analysis showing (**A**) raw data from cyclic creep loading tests and (**B**) residual deformation in unloaded test sample as temperature is increased.

3.2. Mechanics of Vitrimeric Composites at Room and Elevated Temperatures

Advanced polymer-based composites are often exposed to temperatures above room temperature during their lifetime. A limiting factor at such temperatures includes various molecular relaxation mechanisms, such as polymer chain segmental mobility, as well as thermal degradation. To evaluate the mechanical behavior of vitrimeric composites, their mechanical properties such as flexural strength and modulus were measured via three-point bending (3PB) testing at two different temperatures: room temperature and 100 °C. This temperature range was chosen such that the dependence of the mechanical properties of the vitrimeric composites on temperature can be compared and contrasted with the corresponding changes in conventional epoxy composites in the literature [75,76]. The 3PB tests were displacement controlled, and the load applied to the midspan of the sample was monotonically increased until a peak in the load was achieved followed by ~3 mm of extra deflection (corresponding to a maximum tensile strain of ~1.2–1.4%). The applied deflections beyond the peak load were primarily intended to induce damage and plastic deformation in the sample and to subsequently explore the utility of the bond exchanges to recover the initial shape via thermo-mechanical processing.

In the samples that were mechanically loaded at room temperature, the load dropped suddenly when the peak load was reached, due to fiber rupture on the tensile side (Figure 4A). The damage, which mainly occurred during the ~3 mm deflections past the peak load, were studied via optical microscopy. Samples experienced material failure and structural damage (buckling) on the tensile and compressive sides of the sample, respectively, during 3PB testing, as seen from optical images in Figure 4C. On the tensile side (the face that is away from the loading fixture), the surfaces experienced fiber–matrix separation, with some fibers being fractured by the application of high tensile forces. Additionally, matrix cracks were observed on that surface. Conversely, on the compressive side, fibers exhibited breakage, often accompanied by sharp-edged matrix fractures resulting from buckling and fiber deformation away from their straight axis, rather than fiber–matrix separation. However, in the samples that were 3PB-tested at 100 °C, upon reaching the peak load, a gradual decline in the load with displacement was observed, indicative of the sliding between fibers (Figure 4A). The optical images support these findings, as seen in Figure 4C. Comparing initial 3PB tests conducted at room temperature and at elevated temperature, 3PB test analysis reveals that no significant fiber breakage occurred at elevated temperature, since fibers were able to slide during loading.

The flexural strength and modulus of the samples tested at RT and elevated temperature were then estimated from the 3PB load–displacement curves, as presented in Figure 4D,E. The measured strength and modulus of the samples at RT are 888.6 ± 109.2 MPa and 86.03 ± 10.2 GPa, respectively, which is comparable to the properties of advanced composites made with conventional epoxy resins [77,78]. Moreover, the strength and modulus of the samples at RT are ~59% and ~58% higher than the high temperature values, respectively, reflecting the molecular relaxation mechanisms in the matrix at the elevated temperatures. The drop in strength and modulus in our vitrimer composites at elevated temperatures is comparable to those obtained from continuous carbon fiber composites with conventional epoxy matrix [79]. Given the permanent nature of covalent bonds in the conventional epoxy matrix and the dynamic nature of those bonds in ATSP, this favorable comparison reveals the robustness of the exchangeable bonds in our matrix material.

Next, in the plastically deformed three-point bent samples, we studied the utility of the bond exchanges to recover their initial flat shape. For this investigation, the plastically bent samples were subsequently placed in an oven at 280 °C for 2 h at ~0.03 MPa of pressure. As a result of the application of the applied pressure and temperature, the initial shape of the samples (straight bars with no bent) was fully recovered, indicating the significance of bond exchanges in recovering the initial shape of the bars. The images of samples before and after 3PB testing in different temperature conditions as well as the healing setup are seen in Figure 4B. To quantify the extent of the recovery in mechanical properties, the plastically

deformed and subsequently straightened samples were subjected to 3PB tests. Flexural strength and modulus were calculated for these samples before and after healing, as shown in Figure 4D,E.

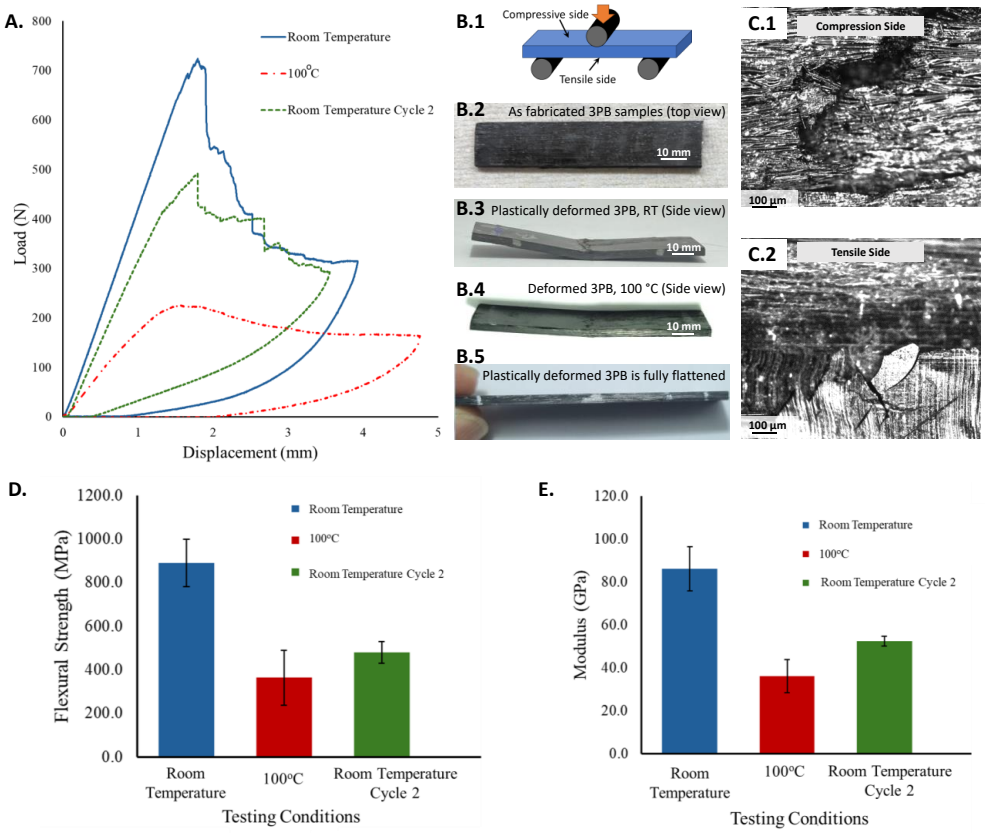

Figure 4. (**A**) Representative load–displacement curves are seen for samples 3PB tested at room temperature, 100 °C, and after one cycle of healing for the room temperature samples. (**B**) (Top) Schematic of 3PB sample is shown. (**B.1**) Schematic of 3PB test, (**B.2**) top view of the as-fabricated sample, (**B.3**) side view of the 3PB sample tested at room temperature, (**B.4**) side view of the 3PB sample tested at 100 °C temperature, (**B.5**) the plastically deformed samples flattened out to their initial shape. (**C**) Digital images of samples before and after 3PB testing and healing with healing set up for room temperature samples shown. (**D**) A graph comparing average flexural strength of 3PB-tested samples is shown. (**E**) A graph comparing average modulus of 3PB-tested samples is shown.

As seen from Figure 4, the strength and modulus of the hot-pressed samples is nearly 50% of the as-fabricated samples. While the full recovery of the initial flat shape is indicative of the role of bond exchange at elevated temperatures that allows for sliding between fibers, the recovery in mechanical properties is only partial, mainly due to nonreversible damages accumulated on the sample, such as fiber failure.

3.3. Mode I Fracture Toughness of Virgin and Healed Vitrimeric Composites

DCB test was conducted on composite samples, and foe each sample it yielded a load vs. displacement curve in a displacement-controlled loading. In this curve, the force initially increased with displacement. Throughout this phase, the crack mouth opened without any apparent crack growth. Following this initial rise, the load rapidly decreased. When synchronizing the data with a video of the DCB testing, this decrease was associated with crack growth as well as a resounding crack noise. After this load drop, the load–displacement curve showed a saw-tooth behavior, corresponding to instances of crack growth and crack arrest [80]. The sample was fully unloaded when the crack grew by ~20 mm from the initial crack length (a_0) of ~54 mm at a rate comperable to the loading

rate. As expected, the accumulated damage on the sample led to a reduced stiffness, such that the zero load corresponds to nearly zero displacement. A representative example of a load–displacement curve with a change in crack length (Δa) for an ATSP CFRP sample is shown in Figure 5.

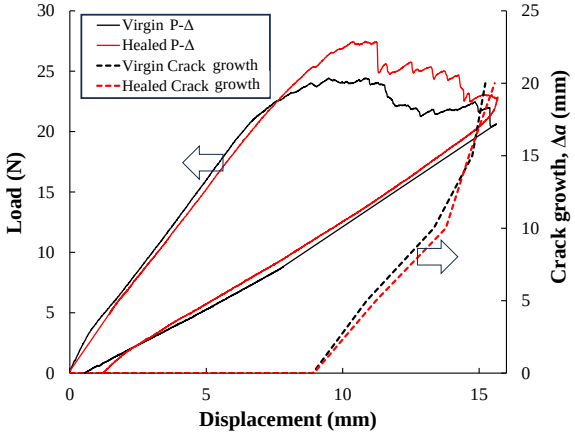

Figure 5. DCB results used for calculating G_{IC} from load vs. displacement and change in crack length of DCB testing before and after a sample was self-healed at 280 °C for 2 h.

After the crack growth, the sample was unmounted, the two faces of the crack were pressed against one another via a grip, and the sample was placed inside an oven at 280 °C for 2 h to complete the healing, at a pressure of ~0.03 MPa. This temperature was chosen as it was above the T_v (~160 °C) after vitrification temperature analysis, as seen in Section 3.1, which is required to trigger the bond exchange and reformation of the crosslinks (Figure 5). The fixtures were mounted onto the healed samples, and the DCB tests were repeated to measure $G_{IC\text{-}h}$.

The fracture toughness of the virgin and healed samples, $G_{IC\text{-}v}$ and $G_{IC\text{-}h}$, respectively, were calculated as discussed in Section 2.5 and compared in Figure 6. Healing efficiency, as the ratio of $G_{IC\text{-}h}$ to $G_{IC\text{-}v}$, was estimated for all samples, as reported in Table S1 (109.48 ± 7.92). Even though the average value of healing efficiency is slightly more than one, the values of $G_{IC\text{-}v}$ and $G_{IC\text{-}h}$ were statistically the same as verified by a t-test with a significance level (α) of 0.05. Here, the t-test null hypothesis is defined as foillows: there is no significant difference between the average $G_{IC\text{-}v}$ and $G_{IC\text{-}h}$. The p-values were calculated by $p = 2 \times (1 - t_{dist}(|t|, df))$ to be ~0.394, where t is the t-statistic, t_{dist} is the cumulative distructation of the t-distribution, and df is degrees of freedom. Therefore, the p-value is much more than 0.05, and the null hypothesis stands. The mechanisms which may lead to slightly higher than unity healing efficiency are explained in Section 3.5.

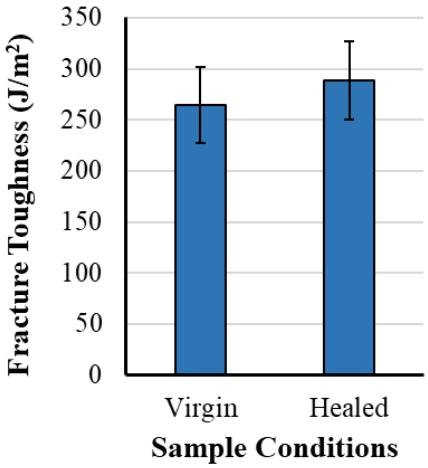

Figure 6. $G_{IC\text{-}v}$ and $G_{IC\text{-}h}$ comparison is shown in the graph.

3.4. Fracture Surface Morphology of DCB Samples

More insight into the healing mechanisms in DCB samples was obtained via investigating the morphology of the samples. To study the fracture surface of ATSP CFRP samples (both the as-fabricated samples and the virgin and self-healed samples), the sample was loaded in the DCB test until the two parts of a sample debonded. The fracture surface was then imaged in SEM. The fractured crack surfaces of the as-fabricated and healed samples were SEM-imaged in the vicinity of the initial crack tip, as shown in the schematic in Figure 7A. The crack path is prominent in the ATSP CFRP samples after DCB testing before self-healing (Figure 7B). Prominent longitudinal intralaminar crack growth is seen in the direction of the carbon fibers in the ATSP CFRP sample. A similar crack path is seen along the direction of the longitudinal crack in the ATSP CFRP sample after DCB testing after self-healing (Figure 7C). After self-healing, the crack path surface and carbon fiber structure are similar to the surface morphology on the as-fabricated ATSP CFRP sample. In both samples, there are observable similar appearances of surface ATSP resin residue and carbon fibers. These surface morphological findings support the effectiveness of the self-healing behavior of ATSP to maintain the integrity of the CFRP sample.

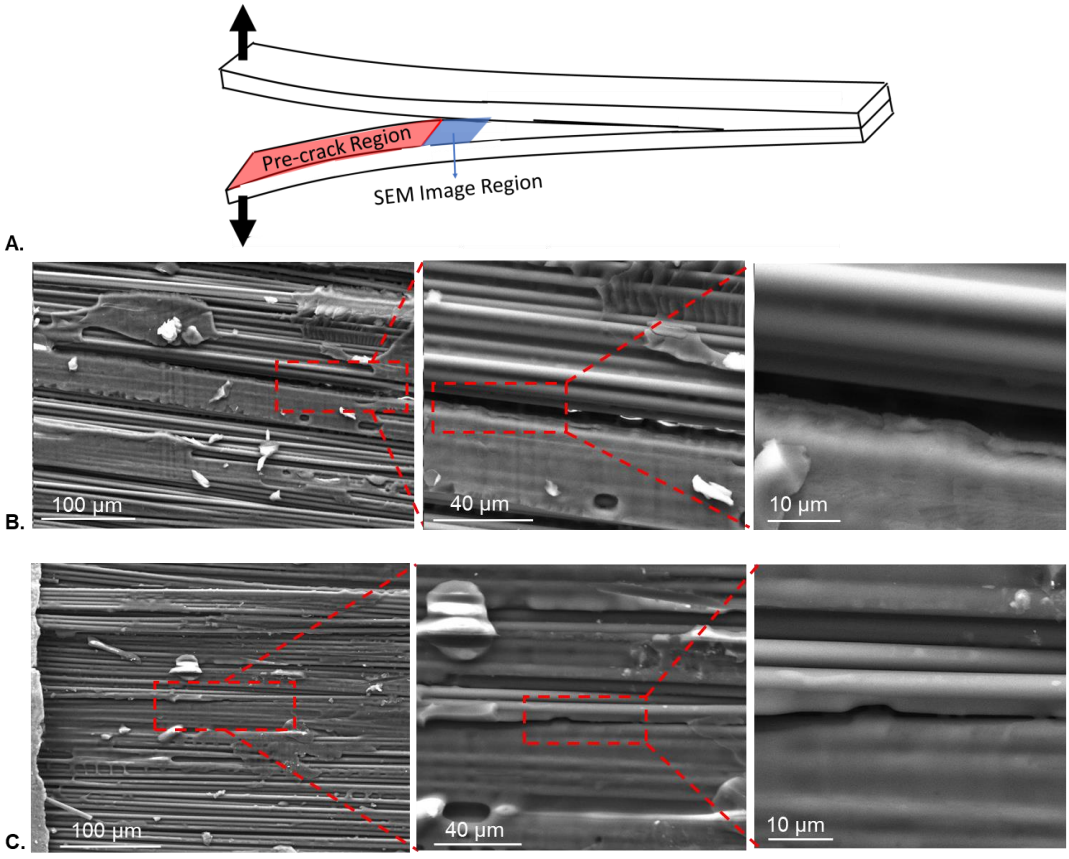

Figure 7. Cross-section SEM images of the fracture surface of ATSP CFRP sample seen in the (**A**) schematic of the fracture surface location (**B**) before self-healing and (**C**) and after self-healing are shown.

3.5. Internal Structure Morphology of DCB Samples

For a more comprehensive understanding of the healing capabilities of ATSP composites, we employed micro-CT X-ray imaging to capture the as-fabricated and self-healed conditions in various planes and locations. The schematics above the micro-CT X-ray images presented in Figure 8A,B provide a visual reference. In the XZ plane (side-view) of both the as-fabricated and self-healed samples comparable pre-crack regions are observed. In the magnified view of the crack tip region in the as-fabricated sample, some voids and gaps are observed in the composite structure, whereas there are fewer voids and gaps in

the healed sample after 280 °C at 2 h (Figure 8A). This finding is very much in line with the slightly higher-than-unity healing efficiency, as discussed in Section 3.1. The presence of voids in the as-fabricated samples may reflect the outgassing from the cure reaction's release of acetic acid from the processing of the virgin samples, which act as a barrier to bonding between composite plies [57]. During DCB testing, the crack mostly grew along the mid-plane of the sample, while the presence of pores may favor slight deviations in crack path, leading to crack growth along the trapped pores. Such crack growth will release volatile species that are trapped in the sample, facilitating the formation of interfacial bonds during subsequent healing. During the healing phase the voids become filled by the self-healing mechanism of ATSP from increased trans-esterification reactions activated by the cure cycle. Thus, the previously weakest available crack surface of the samples is now stronger due to fewer pores for the cracks to propagate along with. It is conceivable to eliminate the manufacturing voids, for instance, by applying higher pressure or longer duration of curing to allow for the volatile species to leave the sample, which is a subject of future studies.

In the front view plane (YZ plane) of the as-fabricated sample, the aluminum foil maintaining the pre-crack area of the sample is observed along with voids and gaps, and the initial compact structure of the composite is seen in the after pre-crack area (Figure 8B). As seen in Figure 8A,B, the cracked area completely healed up to the edge of the pre-crack area in both XZ and YZ planes. The micro-CT X-ray images of as-fabricated and self-healed samples show that the overall structural integrity of the ATSP CFRP samples is restored after self-healing.

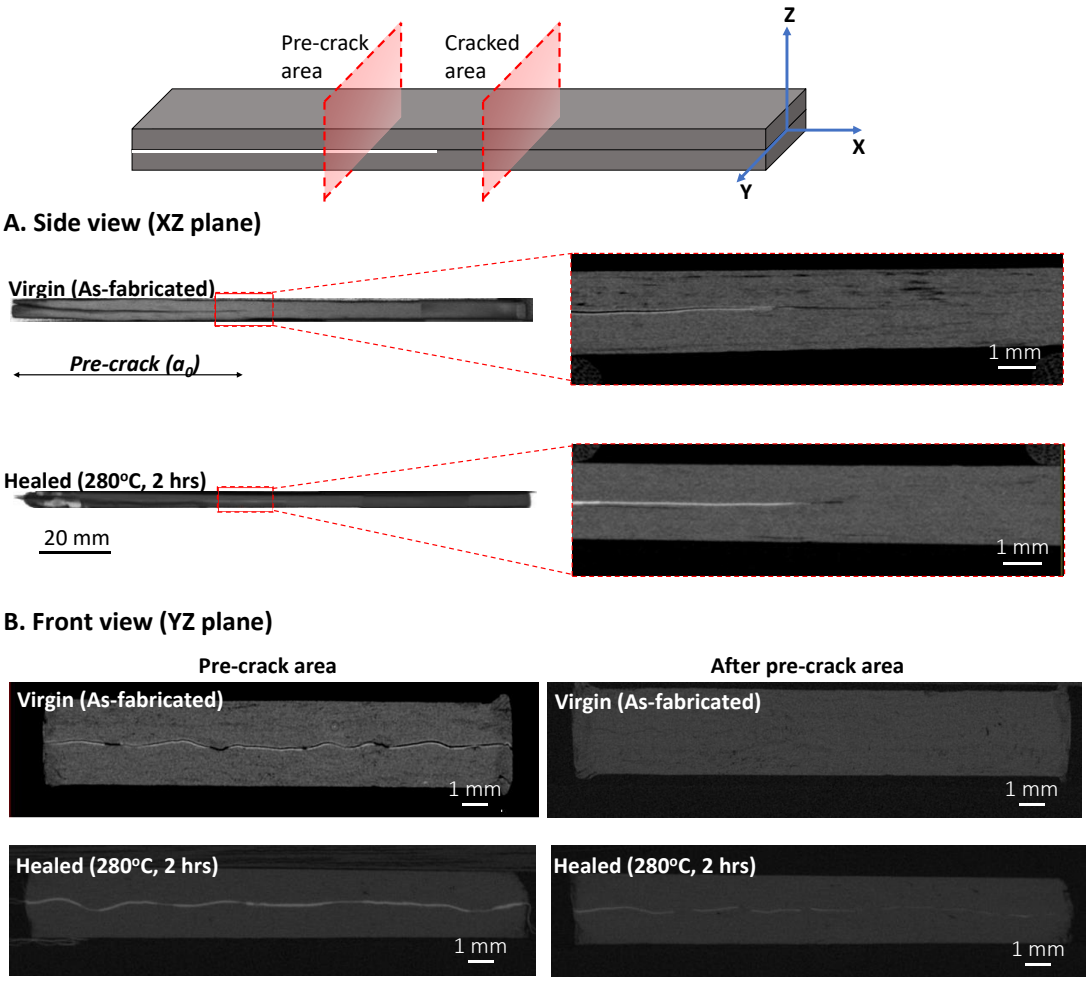

Figure 8. Micro-CT X-ray images of the (**A**) side view (XZ plane) and (**B**) crack plane (YZ plane) are shown of ATSP CFRP samples as fabricated and after self-healing at 280 °C for 2 h.

4. Conclusions

The self-healing mechanical behaviors of ATSP vitrimer composites were studied in both three-point bending and double cantilever beam tests. The healing cycle was composed of heating at 280 °C for 2 h. In all 3PB samples that were plastically deformed, the flat shape of the sample was fully recovered via thermomechanical treatment. After each healing cycle, a reduction in flexural strength and modulus was observed, mainly due to the breakage of the fiber. The restoration of mechanical properties was more successful for samples with less broken fibers for 3PB testing after the second healing cycle. Testing at elevated temperatures reveals that the maximum load did not exceed the breaking limits of the fibers. This is attributed to the sliding mechanism of the fibers within the relatively flexible/softer state of the matrix material (vitrimer), leading to reduced flexural strength compared to testing at ambient temperature.

DCB testing before and after the self-healing of the ATSP CFRP samples demonstrates elevated healing efficiency, which shows the effectiveness of ATSP's self-healing properties. SEM imaging confirms that there is a similar surface morphology of ATSP CFRP samples before and after self-healing. Micro-CT X-ray imaging substantiates the self-healing behavior of ATSP in the samples, since the internal structural morphologies of gaps and voids are decreased after ATSP CFRPs are self-healed. The healing efficiency of all samples was very close to 100%. In some samples, the healing efficiency was barely above 100%. From micro-CT imaging, this was attributed to the removal of the voids in the virgin sample during healing. Despite that, the comparable properties of the healed and virgin fracture toughness suggest that the impacts of voids on the measured properties is very minimal. The presence of the voids was attributed to the outgassing of the ATSP during the curing process. The propagation of cracks enables volatile species to escape from the sample, thereby promoting improved bonding between plies during the healing process. As seen from the results, ATSP has proven to be exceptional by offering self-healing properties that can be used for material repair with various applications in aerospace, medicine, oil and gas, and automotive industries.

Supplementary Materials: The following supporting information can be downloaded at: https://www.mdpi.com/article/10.3390/jcs8070252/s1, Table S1: Average Mode I Fracture Toughness and Average Healing Efficiency.

Author Contributions: The manuscript was written through contributions of all authors. All authors have given approval to the final version of the manuscript. T.M. led the processing and characterization of composites, as well as data analysis, and prepared the first draft of the article; U.O. helped in conducting and analyzing mechanical tests; L.V. characterized the vitrimer; A.A., J.L.M. and A.P. contributed to the discussions of the paper; and M.N. contributed to developing the outline of the work and data analysis. All authors have read and agreed to the published version of the manuscript.

Funding: The authors acknowledge the support from the Air Force Office of Scientific Research (AFOSR) under the award number FA9550-22-1-0496.

Data Availability Statement: The data presented in this study are available upon request to the authors.

Acknowledgments: The authors would like to acknowledge the Texas A&M Microscopy and Imaging Center (MIC), the Micro-CT X-ray Imaging Center at the Texas A&M University Cardiovascular Pathology Laboratory, and the Department of Aerospace Engineering for infrastructural support.

Conflicts of Interest: Author Dr. Jacob L. Meyer was employed by the company ATSP innovations. The remaining authors declare that the research was conducted in the absence of any commercial or financial relationships that could be construed as a potential conflict of interest.

References

1. Yao, S.-S.; Jin, F.-L.; Rhee, K.Y.; Hui, D.; Park, S.-J. Recent advances in carbon-fiber-reinforced thermoplastic composites: A review. *Compos. Part B Eng.* **2018**, *142*, 241–250. [CrossRef]
2. You, J.; Jee, S.M.; Lee, Y.M.; Lee, S.-S.; Park, M.; Kim, T.A.; Park, J.H. Carbon fiber-reinforced polyamide composites with efficient stress transfer via plasma-assisted mechanochemistry. *Compos. Part C Open Access* **2021**, *6*, 100209. [CrossRef]

3. Ozkan, D.; Gok, M.S.; Karaoglanli, A.C. Carbon fiber reinforced polymer (CFRP) composite materials, their characteristic properties, industrial application areas and their machinability. In *Engineering Design Applications III*; Springer: Berlin/Heidelberg, Germany, 2020; pp. 235–253.
4. Kuppusamy, R.R.P.; Rout, S.; Kumar, K. Advanced manufacturing techniques for composite structures used in aerospace industries. In *Modern Manufacturing Processes*; Elsevier: Amsterdam, The Netherlands, 2020; pp. 3–12.
5. Skirbutis, G.; Dzingutė, A.; Masiliūnaitė, V.; Šulcaitė, G.; Žilinskas, J.J. A review of PEEK polymer's properties and its use in prosthodontics. *Stomatologija* **2017**, *19*, 19–23. [PubMed]
6. Chung, D.D. *Composite Materials: Science and Applications*; Springer Science & Business Media: Berlin, Germany, 2010.
7. Mallick, P.K. *Fiber-Reinforced Composites: Materials, Manufacturing, and Design*; CRC Press: Boca Raton, FL, USA, 2007.
8. Jin, F.-L.; Park, S.-J. Preparation and characterization of carbon fiber-reinforced thermosetting composites: A review. *Carbon Lett.* **2015**, *16*, 67–77. [CrossRef]
9. Ozturk, F. Thermoplastic Composite Materials for the Aerospace Industry. *Res. Dev. Mater. Sci.* **2021**, *15*, 1745–1748. [CrossRef]
10. Xu, Y.; Zehnder, A.T. Pressure, hydrolytic degradation and plasticization drive high temperature blistering failure in moisture saturated polyimides. *Extrem. Mech. Lett.* **2017**, *16*, 49–55. [CrossRef]
11. Barbero, E.J. *Introduction to Composite Materials Design*; CRC Press: Boca Raton, FL, USA, 2010.
12. Rao, P.S.; Hardiman, M.; O'Dowd, N.P.; Sebaey, T.A. Comparison of progressive damage between thermoset and thermoplastic CFRP composites under in-situ tensile loading. *J. Compos. Mater.* **2020**, *55*, 1473–1484. [CrossRef]
13. Ivanov, S.G.; Beyens, D.; Gorbatikh, L.; Lomov, S.V. Damage development in woven carbon fibre thermoplastic laminates with PPS and PEEK matrices: A comparative study. *J. Compos. Mater.* **2016**, *51*, 637–647. [CrossRef]
14. Kamble, M.; Vashisth, A.; Yang, H.; Pranompont, S.; Picu, C.R.; Wang, D.; Koratkar, N. Reversing fatigue in carbon-fiber reinforced vitrimer composites. *Carbon* **2022**, *187*, 108–114. [CrossRef]
15. Yang, Y.; Ding, X.; Urban, M.W. Chemical and physical aspects of self-healing materials. *Prog. Polym. Sci.* **2015**, *49*, 34–59. [CrossRef]
16. Yang, Y.; Urban, M.W. Self-healing polymeric materials. *Chem. Soc. Rev.* **2013**, *42*, 7446–7467. [CrossRef] [PubMed]
17. Garcia, S.J. Effect of polymer architecture on the intrinsic self-healing character of polymers. *Eur. Polym. J.* **2014**, *53*, 118–125. [CrossRef]
18. Jud, K.; Kausch, H.; Williams, J. Fracture mechanics studies of crack healing and welding of polymers. *J. Mater. Sci.* **1981**, *16*, 204–210. [CrossRef]
19. Lu, L.; Fan, J.; Li, G.J.P. Intrinsic healable and recyclable thermoset epoxy based on shape memory effect and transesterification reaction. *Polymer* **2016**, *105*, 10–18. [CrossRef]
20. Hornat, C.C.; Urban, M.W. Shape memory effects in self-healing polymers. *Prog. Polym. Sci.* **2020**, *102*, 101208. [CrossRef]
21. Abend, M.; Zechel, S.; Schubert, U.S.; Hager, M.D. Detailed Analysis of the Influencing Parameters on the Self-Healing Behavior of Dynamic Urea-Crosslinked Poly (methacrylate) s. *Molecules* **2019**, *24*, 3597. [CrossRef] [PubMed]
22. Sumerlin, B.S. Next-generation self-healing materials. *Science* **2018**, *362*, 150–151. [CrossRef] [PubMed]
23. Williams, G.; Trask, R.; Bond, I. A self-healing carbon fibre reinforced polymer for aerospace applications. *Compos. Part A Appl. Sci. Manuf.* **2007**, *38*, 1525–1532. [CrossRef]
24. Kontiza, A.; Semitekolos, D.; Milickovic, T.K.; Pappas, P.; Koutroumanis, N.; Galiotis, C.; Charitidis, C.A. Double cantilever beam test and micro-computed tomography as evaluation tools for self-healing of CFRPs loaded with DCPD microcapsules. *Compos. Struct.* **2022**, *279*, 114780. [CrossRef]
25. Lemmens, R.J.; Dai, Q.; Meng, D.D.; Mechanics, A.F. Side-groove influenced parameters for determining fracture toughness of self-healing composites using a tapered double cantilever beam specimen. *Theor. Appl. Fract. Mech.* **2014**, *74*, 23–29. [CrossRef]
26. Benazzo, F.; Rigamonti, D.; Sala, G.; Grande, A.M. A critical appraisal of fracture mechanics methods for self-healing and healable composites characterization. *Compos. Part A Appl. Sci. Manuf.* **2023**, *167*, 107450. [CrossRef]
27. Cho, S.H.; Andersson, H.M.; White, S.R.; Sottos, N.R.; Braun, P.V. Polydimethylsiloxane-based self-healing materials. *Adv. Mater.* **2006**, *18*, 997–1000. [CrossRef]
28. Romero-Sabat, G.; Gago-Benedí, E.; Roa Rovira, J.J.; González-Gálvez, D.; Mateo, A.; Medel, S.; Tolentino Chivite, A. Development of a highly efficient extrinsic and autonomous self-healing polymeric system at low and ultra-low temperatures for high-performance applications. *Compos. Part A Appl. Sci. Manuf.* **2021**, *145*, 106335. [CrossRef]
29. Thies, C. *Microencapsulation*; Wiley: Hoboken, NJ, USA, 2005. [CrossRef]
30. Jones, A.S.; Rule, J.D.; Moore, J.S.; White, S.R.; Sottos, N.R. Catalyst morphology and dissolution kinetics of self-healing polymers. *Chem. Mater.* **2006**, *18*, 1312–1317. [CrossRef]
31. Shansky, E. *Synthesis and Characterization of Microcapsules for Self-Healing Materials*; Department of Chemistry Indiana University: Bloomington, IN, USA, 2005.
32. Dry, C. Procedures developed for self-repair of polymer matrix composite materials. *Compos. Struct.* **1996**, *35*, 263–269. [CrossRef]
33. Dry, C.M. Adhesive liquid core optical fibers for crack detection and repairs in polymer and concrete matrices. *Smart Struct. Mater. 1995 Smart Sens. Process. Instrum.* **1995**, *2444*, 410–413.
34. Dry, C.M.; McMillan, W. Crack and damage assessment in concrete and polymer matrices using liquids released internally from hollow optical fibers. *Smart Struct. Mater. 1996 Smart Sens. Process. Instrum.* **1996**, *2718*, 448–451.

35. Dry, C.M.; Sottos, N.R. Passive smart self-repair in polymer matrix composite materials. *Smart Struct. Mater. 1993 Smart Mater.* **1993**, *1916*, 438–444.
36. Motuku, M.; Vaidya, U.; Janowski, G. Parametric studies on self-repairing approaches for resin infused composites subjected to low velocity impact. *Smart Mater. Struct.* **1999**, *8*, 623. [CrossRef]
37. Bleay, S.M.; Loader, C.B.; Hawyes, V.; Humberstone, L.; Curtis, P. A smart repair system for polymer matrix composites. *Compos. Part A Appl. Sci. Manuf.* **2001**, *32*, 1767–1776. [CrossRef]
38. Hucker, M.; Bond, I.; Foreman, A.; Hudd, J. Optimisation of hollow glass fibres and their composites. *Adv. Compos. Lett.* **1999**, *8*, 096369359900800406. [CrossRef]
39. Trask, R.; Bond, I. Biomimetic self-healing of advanced composite structures using hollow glass fibres. *Smart Mater. Struct.* **2006**, *15*, 704. [CrossRef]
40. Pang, J.; Bond, I. 'Bleeding composites'—Damage detection and self-repair using a biomimetic approach. *Compos. Part A Appl. Sci. Manuf.* **2005**, *36*, 183–188. [CrossRef]
41. Pang, J.W.; Bond, I.P. A hollow fibre reinforced polymer composite encompassing self-healing and enhanced damage visibility. *Compos. Sci. Technol.* **2005**, *65*, 1791–1799. [CrossRef]
42. Williams, H.R.; Trask, R.S.; Bond, I.P. Self-healing composite sandwich structures. *Smart Mater. Struct.* **2007**, *16*, 1198. [CrossRef]
43. Sanada, K.; Yasuda, I.; Shindo, Y. Transverse tensile strengh of unidirectional fiber-reinforced polymers and self-healing of interfacial debonding. *Plast. Rubber Compos.* **2006**, *35*, 67–72. [CrossRef]
44. Zhang, M.Q.; Rong, M.Z. *Extrinsic and Intrinsic Approaches to Self-Healing Polymers and Polymer Composites*; John Wiley & Sons: Hoboken, NJ, USA, 2022.
45. Frich, D.; Goranov, K.; Schneggenburger, L.; Economy, J. Novel high-temperature aromatic copolyester thermosets: Synthesis, characterization, and physical properties. *Macromolecules* **1996**, *29*, 7734–7739. [CrossRef]
46. Frich, D.; Economy, J.; Goranov, K. Aromatic copolyester thermosets: High temperature adhesive properties. *Polym. Eng. Sci.* **1997**, *37*, 541–548. [CrossRef]
47. Montarnal, D.; Capelot, M.; Tournilhac, F.; Leibler, L. Silica-like malleable materials from permanent organic networks. *Science* **2011**, *334*, 965–968. [CrossRef]
48. Yang, Y.; Xu, Y.; Ji, Y.; Wei, Y.J. Functional epoxy vitrimers and composites. *Prog. Mater. Sci.* **2021**, *120*, 100710. [CrossRef]
49. Zheng, J.; Png, Z.M.; Ng, S.H.; Tham, G.X.; Ye, E.; Goh, S.S.; Loh, X.J.; Li, Z.J. Vitrimers: Current research trends and their emerging applications. *Mater. Today* **2021**, *51*, 586–625. [CrossRef]
50. Shi, Q.; Yu, K.; Kuang, X.; Mu, X.; Dunn, C.; Dunn, M.; Wang, T.; Qi, H. Recyclable 3D Printing of Vitrimer Epoxy. *Mater. Horiz.* **2017**, *4*, 598–607. [CrossRef]
51. Zheng, N.; Xu, Y.; Zhao, Q.; Xie, T. Dynamic Covalent Polymer Networks: A Molecular Platform for Designing Functions beyond Chemical Recycling and Self-Healing. *Chem. Rev.* **2021**, *121*, 1716–1745. [CrossRef] [PubMed]
52. Hubbard, A.M.; Ren, Y.; Konkolewicz, D.; Sarvestani, A.; Picu, C.R.; Kedziora, G.S.; Roy, A.; Varshney, V.; Nepal, D. Vitrimer Transition Temperature Identification: Coupling Various Thermomechanical Methodologies. *ACS Appl. Polym. Mater.* **2021**, *3*, 1756–1766. [CrossRef]
53. Sharma, H.; Rana, S.; Singh, P.; Hayashi, M.; Binder, W.H.; Rossegger, E.; Kumar, A.; Schlögl, S. Self-healable fiber-reinforced vitrimer composites: Overview and future prospects. *RSC Adv.* **2022**, *12*, 32569–32582. [CrossRef] [PubMed]
54. Palmieri, B.; Cilento, F.; Amendola, E.; Valente, T.; Dello Iacono, S.; Giordano, M.; Martone, A. An Investigation of the Healing Efficiency of Epoxy Vitrimer Composites Based on Zn^{2+} Catalyst. *Polymers* **2023**, *15*, 3611. [CrossRef] [PubMed]
55. Zhao, Y.; Zhao, M.; Wang, A.; Chang, Z.; Wang, Z.; Zhang, K. Experimental study on the mode I interlaminar properties of self-healable vitrimeric CFRP with various interfaces. *Compos. Part B Eng.* **2023**, *261*, 110806. [CrossRef]
56. Bakir, M.; Elhebeary, M.; Meyer, J.L.; Sutrisno, A.; Economy, J.; Jasiuk, I.J. Interfacial liquid crystalline mesophase domain on carbon nanofillers in aromatic thermosetting copolyester matrix. *J. Appl. Polym. Sci.* **2018**, *135*, 46584. [CrossRef]
57. Vaezian, B.; Meyer, J.L.; Economy, J. Processing of aromatic thermosetting copolyesters into foams and bulk parts: Characterization and mechanical properties. *Polym. Adv. Technol.* **2016**, *27*, 1006–1013. [CrossRef]
58. Meyer, J.L.; Lan, P.; Bakir, M.; Jasiuk, I.; Economy, J. Wide Area Reversible Adhesive for In-Space Assembly. *Macromol. Mater. Eng.* **2020**, *305*, 2000006. [CrossRef]
59. Bashandeh, K.; Lan, P.; Meyer, J.L.; Polycarpou, A.A. Tribological Performance of Graphene and PTFE Solid Lubricants for Polymer Coatings at Elevated Temperatures. *Tribol. Lett.* **2019**, *67*, 99. [CrossRef]
60. Frich, D.; Hall, A.; Economy, J.J. Nature of adhesive bonding via interchain transesterification reactions (ITR). *Macromol. Chem. Phys.* **1998**, *199*, 913–921. [CrossRef]
61. Meyer, J.L.; Bakir, M.; Lan, P.; Economy, J.; Jasiuk, I.; Bonhomme, G.; Polycarpou, A.A. Reversible Bonding of Aromatic Thermosetting Copolyesters for In-Space Assembly. *Macromol. Mater. Eng.* **2019**, *304*, 1800647. [CrossRef]
62. Taynton, P.; Zhu, C.; Loob, S.; Shoemaker, R.; Pritchard, J.; Jin, Y.; Zhang, W. Re-healable polyimine thermosets: Polymer composition and moisture sensitivity. *Polym. Chem.* **2016**, *7*, 7052–7056. [CrossRef]
63. Chao, A.; Negulescu, I.; Zhang, D. Dynamic covalent polymer networks based on degenerative imine bond exchange: Tuning the malleability and self-healing properties by solvent. *Macromolecules* **2016**, *49*, 6277–6284. [CrossRef]
64. Boutelle, R.C.; Northrop, B.H. Substituent effects on the reversibility of furan–maleimide cycloadditions. *J. Org. Chem.* **2011**, *76*, 7994–8002. [CrossRef] [PubMed]

65. Schneggenburger, L.; Osenar, P.; Economy, J. Direct evidence for sequence ordering of random semicrystalline copolyesters during high-temperature annealing. *Macromolecules* **1997**, *30*, 3754–3758. [CrossRef]
66. Stevens, M.P. *Polymer Chemistry: An Introduction*; Oxford University Press: Oxford, UK, 1999.
67. Mangalgiri, P.J. Polymer-matrix composites for high-temperature applications. *Def. Sci. J.* **2005**, *55*, 175. [CrossRef]
68. Bashandeh, K.; Lan, P.; Polycarpou, A.A. Tribology of self-lubricating high performance ATSP, PI, and PEEK-based polymer composites up to 300 °C. *Friction* **2023**, *11*, 141–153. [CrossRef]
69. Krull, B.; Patrick, J.; Hart, K.; White, S.; Sottos, N. Automatic optical crack tracking for double cantilever beam specimens. *Exp. Tech.* **2016**, *40*, 937–945. [CrossRef]
70. Hashemi, S.M.K.; Kinloch, A.J.; Williams, J.G. Corrections needed in double-cantilever beam tests for assessing the interlaminar failure of fibre-composites. *J. Mater. Sci. Lett.* **1989**, *8*, 125–129. [CrossRef]
71. Snyder, A.; Phillips, Z.; Turicek, J.; Diesendruck, C.; Nakshatrala, K.; Patrick, J. Prolonged in situ self-healing in structural composites via thermo-reversible entanglement. *Nat. Commun.* **2022**, *13*, 6511. [CrossRef] [PubMed]
72. Lan, P.; Polychronopoulou, K.; Zhang, Y.; Polycarpou, A.A. Three-body abrasive wear by (silica) sand of advanced polymeric coatings for tilting pad bearings. *Wear* **2017**, *382*, 40–50. [CrossRef]
73. Lan, P.; Zhang, Y.; Dai, W.; Polycarpou, A.A. A phenomenological elevated temperature friction model for viscoelastic polymer coatings based on nanoindentation. *Tribol. Int.* **2018**, *119*, 299–307. [CrossRef]
74. Lei, Y.; Wang, Y.; Yuan, A.; Zhao, S.; Chen, Y.; Xiao, Y.; Jiang, L.; Lei, J. Solving the difficult recyclability of conventional thermosetting polyurea elastomers based on commercial raw materials in a facile way. *J. Mater. Chem. A* **2022**, *10*, 6713–6723. [CrossRef]
75. Mulqueen, D.W.; Sattar, S.; Kravchenko, O.G. Mechanical and thermal properties of carbon fiber epoxy composite with interlaminar graphene at elevated temperature. *Compos. Part B Eng.* **2023**, *255*, 110609. [CrossRef]
76. Mani, D.; Vu, M.C.; Jeong, T.-H.; Kim, J.-B.; Lim, C.-S.; Lim, J.-H.; Kim, K.-M.; Kim, S.-R. 3D structured graphene fluoride-based epoxy composites with high thermal conductivity and electrical insulation. *Compos. Part A Appl. Sci. Manuf.* **2021**, *149*, 106585. [CrossRef]
77. Kim, S.G.; Heo, S.J.; Kim, S.; Kim, J.; Kim, S.O.; Lee, D.; Lee, S.; Kim, J.; You, N.-H.; Kim, M.; et al. Ultrahigh strength and modulus of polyimide-carbon nanotube based carbon and graphitic fibers with superior electrical and thermal conductivities for advanced composite applications. *Compos. Part B Eng.* **2022**, *247*, 110342. [CrossRef]
78. Chae, H.G.; Newcomb, B.A.; Gulgunje, P.V.; Liu, Y.; Gupta, K.K.; Kamath, M.G.; Lyons, K.M.; Ghoshal, S.; Pramanik, C.; Giannuzzi, L. High strength and high modulus carbon fibers. *Carbon* **2015**, *93*, 81–87. [CrossRef]
79. Wen, J.; Wu, Y.; Hou, X.; Yan, M.; Xiao, Y. Effect of high temperature on mechanical properties and porosity of carbon fiber/epoxy composites. *J. Reinf. Plast. Compos.* **2022**, *42*, 990–1005. [CrossRef]
80. Carlsson, L.A.; Adams, D.F.; Pipes, R.B. *Experimental Characterization of Advanced Composite Materials*; CRC Press: Boca Raton, FL, USA, 2014.